

# EXTRACTION OF DAMAGED BUILDINGS DUE TO THE 2011 TOHOKU, JAPAN EARTHQUAKE TSUNAMI

Wen Liu<sup>1)</sup>, Fumio Yamazaki<sup>1)</sup>, Hideomi Gokon<sup>2)</sup> and Shunichi Koshimura<sup>2)</sup>

<sup>1)</sup> Department of Urban Environment Systems, Chiba University, Japan

<sup>2)</sup> International Research Institute of Disaster Science, Tohoku University, Japan

## ABSTRACT

The 11 March 2011 Tohoku, Japan earthquake caused gigantic tsunamis and widespread devastations. Various satellites quickly captured the details of affected areas, and were used for emergency response. In this study, high-resolution pre- and post-event TerraSAR-X (TSX) intensity images were used to identify damaged buildings. Since the damaged buildings show changes in backscattering intensity, they can be detected by calculating the difference. A GIS map was introduced to identify individual damaged buildings and investigate their characteristics. According to the side-looking nature of SAR sensors, the buildings' shapes obtained from the GIS map were converted to match their locations in the TSX images. Then washed-away and damaged buildings were extracted using the changed area of SAR intensity within a building's wall and outline. The results were compared with visual interpretation results, and the accuracy of the proposed method was confirmed.

*Index Terms*—tsunami, radar, buildings, feature extraction, loss measurement

## 1. INTRODUCTION

The Tohoku earthquake with the  $M_w$  9.0 hit Japan on March 11, 2011. The epicenter was located at  $38.322^\circ$  N,  $142.369^\circ$  E at a depth of about 32 km. The earthquake triggered extremely high tsunamis of up to 40.5 m run-up in Miyako, Iwate Prefecture, and caused huge loss of human lives and destruction of infrastructure. According to the Geospatial Information Authority of Japan (GSI), the areas totaling approximately  $561 \text{ km}^2$  were flooded by tsunamis following the earthquake [1].

Remote sensing is an efficient tool to monitor a wide range of natural events by optical and radar sensors. Although optical images can easily capture detailed ground surface information, the approach is restricted by weather conditions. In contrast, synthetic aperture radar (SAR) sensing is independent of weather and daylight conditions, and thus more suitable for mapping damaged areas reliably and promptly. Due to remarkable improvements in radar

sensors, high-resolution COSMO-SkyMed and TerraSAR-X (TSX) SAR images are available with ground resolution of 1 to 5 m, providing detailed surface information.

SAR images have also been used to investigate damage to buildings by interferometric analysis or calculating intensity changes [2-3]. Recently, several studies attempted to detect damage at the scale of a single building unit, using both high-resolution optical and SAR images [4-5].

In this study, a pre-event and a post-event TSX intensity images were used to identify damaged buildings following the Tohoku earthquake tsunami. Washed-away and damaged buildings were distinguished by the areal ratio of SAR intensity change within a building. A GIS map was then introduced to identify each damaged building [6]. Finally, the accuracy of the proposed method was assessed through comparison with the GIS map and aerial photographs.

## 2. SAR IMAGES AND PRE-PROCESSING

This study focuses on the coastal zone of Tohoku, Japan, shown in Fig. 1(a), which was most severely affected in the 2011 Tohoku earthquake tsunami. It contains about  $55 \text{ km}^2$  areas. According to the result of visual interpretation conducted by Gokon and Koshimura, which is shown in Fig. 2, more than 30 thousands building existed before the tsunami and about 3 thousands buildings out of them were washed away [6]. Two TSX images, taken before and after the earthquake, were used to detect damaged buildings, which are shown in Fig. 1(b-c). The pre-event image was taken on October 21, 2010 with  $37.3^\circ$  incident angle, and the post-event image was taken on March 13 (two days after the earthquake) with the same incidence angle at the center of the image. Those images were captured with HH polarization and in a descending path. The images were acquired in the StripMap mode, and thus both the azimuth and ground range resolutions were about 3.3 m. We used the orthorectified multi-look corrected products (EEC) produced by DLR, where the image distortion caused by a variable terrain height was compensated for by using a globally available DEM (SRTM). The products were provided in the form projected to a WGS84 reference ellipsoid with a resampled square pixel size of 1.25 m.

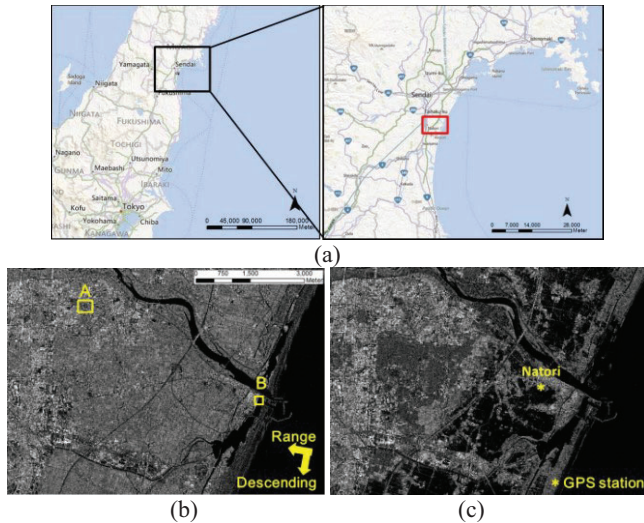


Fig. 1. Study area along the Pacific coast of Tohoku, Japan (a); the pre-event TSX image taken on Oct. 21, 2010 (b) and the post-event image taken on March 13, 2011 (c)

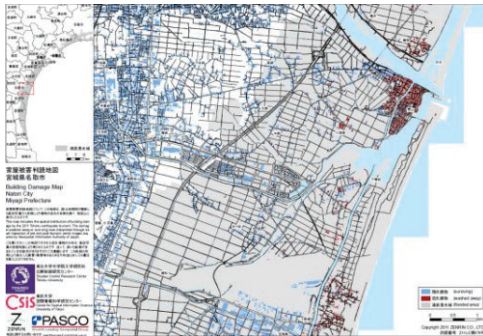


Fig. 2. Building Damage Map of Natori City produced by Gokon and Koshimura using GIS data and aerial photographs taken after the earthquake [6].

### 3. CRUSTAL MOVEMENTS

According to the GPS Earth Observation Network System (GEONET) operated by GSI, crustal movements exceeded 5.3 m horizontally, and 1.2 m vertically over wide areas of the Tohoku region. Since the TSX images used in this study were geo-coded by the GPS orbit determination to a high level of accuracy [7], the displacements occurred between the pre- and post-event TSX images due to the crustal movements. These displacements were used to detect crustal movements [8], but they will cause errors when detecting changes associated with damaged buildings in this study.

According to the GPS records from the Natori ground control station in the study area, which is shown in Fig. 1(c), 3.18 m southeast horizontal and 0.25 m downward movements were observed until March 12, 2011. The three-dimensional surface displacements recorded at the GPS station were converted to the two-dimensional displacements in the TSX images considering the side-looking observation mode of SAR, which are 2.73 m to the east and 0.61 m to the south. Then the pre-event TSX image was manually

shifted 2 pixels (2.5 m) to the east (to the right in the figure) in order to match the post-event TSX image.

### 4. CONVERSION OF BUILDING'S SHAPE

Building damage can be detected by the amount of change in a building's outline. However, the outlines of buildings in the GIS map did not match those in the TSX images, due to the side-looking nature of SAR. A building in a TSX image shows layover from the actual position to the direction of the sensor, as shown in Fig. 3(a). The layover is proportional to the building height, as in Eq. 1.

$$L = H / \tan\theta \quad (1)$$

where  $\theta$  is the incident angle of the radar beam.

Fig. 3(c) shows the outlines of buildings over the pre-event image. The walls of a building, which show highest backscatter due to corner reflection, are outside the outline in the GIS map. In this case, the building cannot be detected as damaged even when a large change occurs to its walls. Therefore, the building shapes in the GIS map were expanded to the direction of the SAR sensor (southeast) in order to match those in the TSX images. Since the height data for buildings were not available, all the buildings in the study area were considered as two-storied with 6-m height according to the local information. The layover was then approximately 7.9 m, as calculated from the  $37.3^\circ$  incidence angle. The path of TSX was  $190.4^\circ$  clockwise from north, which means that the layover can be decomposed into 7.8 m to the east and 1.4 m to the south. Hence, the GIS map was shifted 7 pixels to the east and 2 pixels to the south first. Then the original shape and the shifted shape were merged to new building outlines, as shown in Fig. 3(b). When two neighboring buildings were located much close along the range direction, the expand shape of the farther one overlaps on the shape of the nearer one. Finally, the new building outlines, after conversion, were plotted on the pre-event TSX image, as shown in Fig. 3(d). Since all the buildings were considered as 6-m height, several shapes of buildings with the different heights were still not matched. However, compared with Fig. 3(c), most parts of high backscattering intensities were located within the new building outlines.

### 5. DAMAGE DETECTION

Considering to the resolution of the TSX images and the sizes of ordinary houses, the buildings smaller than  $40 \text{ m}^2$  were removed from the targets. Then there remain about 25 thousands buildings in the study area.

Before damage extraction, the characteristics of damaged buildings in the TSX images were investigated. Fig. 4 shows one part of an inundated area over the frame B of Fig. 1(b). All the buildings except one were completely washed away. From the color composite of the pre- and post-event TSX images, shown in Fig. 4(c), the high

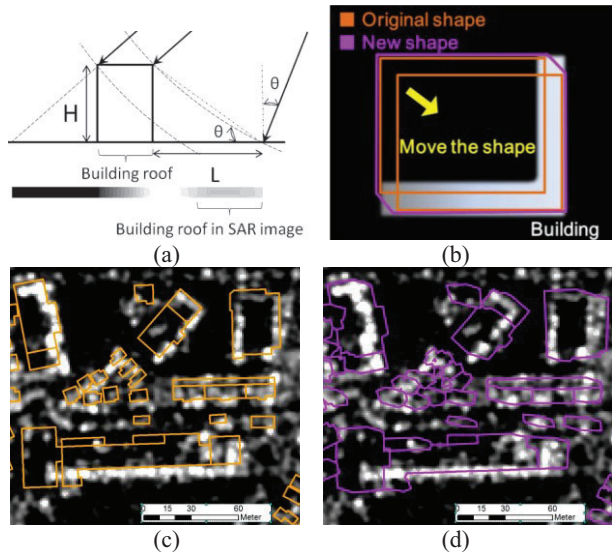


Fig. 3. Schematic figure of a building's location in a SAR image (a), and the shift of the building's shape (b); the GIS map of buildings over the pre-event TSX image (b) over the frame A of Fig. 1.(b), and the new result after shifting the building shapes (c).

backscatter areas of the washed away buildings were shown almost in Cyan color, which means the backscatter completely decreased. A survived building, which is shown in a yellow frame, seems no damage from an aerial photograph. However, the damage to its walls can be confirmed from the ground photos. Parts of the high backscatter areas decreased due to reduced corner reflection from the walls, and the other parts still show high backscatter. Thus, the percentage of change in the backscattering intensity of building walls can be used to distinguish washed-away buildings and damaged buildings.

### 5.1. Damaged walls detection

The areas of building walls were extracted from the pre-event TSX image. Since walls always show the highest backscatter in a building's outline, they can be extracted by calculating the mean value ( $\mu$ ) and standard deviation ( $\sigma$ ) within the building's outline. The areas in the outline of a building with the backscattering intensity greater than  $\mu + 0.5\sigma$  were extracted as walls. A part of the result at the same location of Fig. 4 is shown in Fig. 5(a).

Then the changes in the walls were detected by calculating the difference between the pre- and post-event TSX intensity images. Since the standard deviation of walls outside inundation was 4.6 dB, the difference greater than  $\pm 5.0$  dB was considered as changes. Both for washed-away and damaged cases, the backscatter of walls decreased. Thus, the walls with the difference less than  $-5.0$  dB were considered as damaged. The percentage of damaged pixels within the walls of a building was calculated.

When a building was washed away, a small part of the walls was left. Thus, a building with the percentage of decrease greater than 61% was classified as washed away.

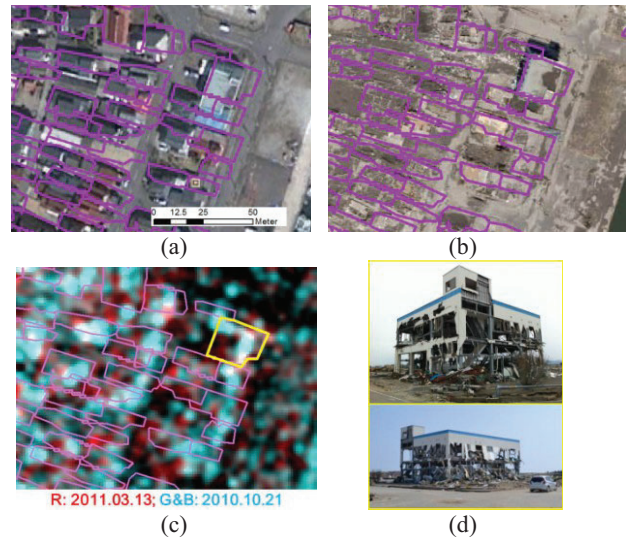


Fig. 4. Aerial photographs taken on March 31, 2010 over the frame B of Fig. 1(b), obtained from Google Earth (a), and taken on March 13, 2011 by GSI (b); the color composite of the pre- and post-event TSX intensity images (c); ground photos cited from website of Yahoo [9].

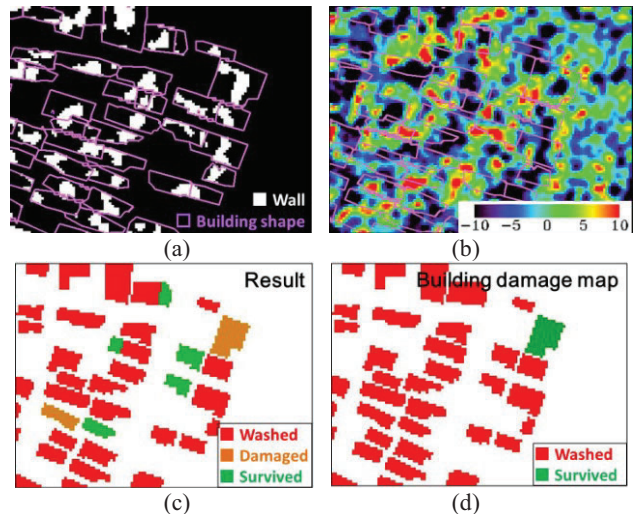


Fig. 5. Result of wall extraction (a); difference image between the pre- and post-event TSX images (b); result of damage classification (c) and damage building map cited from [6] (d).

Although the pre-event image has been shifted to cancel the crustal movements, some differences still remain between the buildings' locations of the pre- and post-event TSX images. Therefore, the change percentage for a non-change building was not equal to zero, especially in the eastern zone. Then a building with the change percentage less than 50% was classified as no damage, and the one with the percentage between 51% and 60% was classified as damaged.

### 5.2. Debris detection

Since the SAR sensor observed from the southeast direction by side-looking, the wall of a building close to its front nearby building along the range direction cannot be

observed in the SAR image. Thus, the buildings in the second row from the sensor direction show low backscatter without corner reflection. The changes of these buildings cannot be detected by focusing on walls. Therefore, debris with increasing backscatter was also extracted in this study to improve the accuracy of damage extraction.

When a building was completely collapsed, its debris might remain at the location of radar shadow or the roof in the pre-event image, which makes the backscatter to increase. These changes might occur in the areas which were not walls (with low backscatter), and can be used to detect the washed away buildings. Then the non-wall areas with the backscatter increase greater than 5.0 dB were seen as debris, and their percentages were calculated. Considering to the effect of crustal movements, a building with the percentage of debris greater than 55% was classified as washed away.

### 5.3. Result of damage detection

A part of the result by integrating damaged walls and debris was shown in Fig. 5(c). Compared with the result of visual interpretation which is shown in Fig. 5(d), most washed buildings were classified accurately. Although omission errors have been reduced by including debris, several washed buildings behind other buildings still could not be detected. However, seriously damaged buildings, like one shown in Fig. 4, can be recognized.

The accuracy of damage extraction was calculated by introducing the building damage map as a reference, and is shown in Table I. When the result was evaluated by pixel-base, the overall accuracy in the study area was 95%, with the producer accuracy of 65% and the user accuracy of 67% for washed buildings. The Kappa coefficient between the result and the reference was 0.63. When the result was evaluated by building unit-base, the overall accuracy was 93%, the producer accuracy was 62% and the user accuracy was 61%. 827 buildings were classified as damaged by the proposed method, and 215 of which were judged as survived by visual interpretation using aerial photographs. Washed buildings were misclassified as damaged due to the low decrease of backscatter caused by debris. The other reason for classification errors was discrepancy between the real locations of buildings and those in the TSX images. Since all the buildings in the study area were as assumed to be 6 m high, the outlines of one-storied or three-storied buildings were not matched with those in the TSX images. Thus, some damaged buildings of these types could not be detected.

## 6. CONCLUSION

In this study, building damage following the 2011 Tohoku, Japan earthquake tsunami was assessed using high-resolution TerraSAR-X intensity images taken before and after the event. Damaged and washed-away buildings were detected from the changes of backscattering coefficients. The percentage of pixels with decreased intensity within the

Table I. Accuracy of damage detection evaluated by pixel-base (a) and building unit-base (b) methods.

		(a)			
pixel-base		Building Damage Map (%)			
		Washed	Survived	Total	U. A.
Detected result	Washed	5.0	2.5	7.5	66.7
	Damaged and non-change	2.7	89.7	92.5	97.1
	Total	7.8	92.2	100.0	
	P. A.	64.9	89.7		94.8
		(b)			
Building unit-base		Building Damage Map			
		Washed	Survived	Total	U. A.
Detected result	Washed	1,378	885	2,263	60.9%
	Damaged and non-change	832	21,150	21,982	96.2%
	Total	2,210	22,035	24,245	
	P. A.	62.4%	96.0%		92.9%

walls and that of increased intensity outside walls in the outline of each building was calculated and used to judge its damage status. The resulting damage classification was compared with a GIS damage map produced by visual interpretation, showing that the proposed method achieved 90% overall accuracy. Thus, the proposed approach using high-resolution SAR images is considered to be useful in emergency response following natural disasters.

## 7. REFERENCES

The TerraSAR-X images used in this study were provided by PASCO Corporation, Tokyo, Japan as one of the granted projects of the SAR data application research committee.

## 8. REFERENCES

- [1] Geospatial Information Authority of Japan (GSI), 2001. [http://www.gsi.go.jp/BOUSAI/h23\\_tohoku.html](http://www.gsi.go.jp/BOUSAI/h23_tohoku.html).
- [2] Y. Ito, M. Hosokawa, H. Lee, and J.G. Liu, "Extraction of damaged regions using SAR data and neural networks," *ISPRS2000, XXXIII-B1*, pp. 156–163, 2000.
- [3] M. Matsuoka, and F. Yamazaki, "Building damage mapping of the 2003 Bam, Iran, Earthquake using Envisat/ASAR intensity imagery," *Earthquake Spectra*, 21, pp. S285–S294, 2005.
- [4] D. Brunner, G. Lemoine, and L. Bruzzone, "Earthquake damage assessment of buildings using VHR optical and SAR imagery," *IEEE Transactions on Geoscience and Remote Sensing*, 48(5), pp. 2403–2420, 2010.
- [5] T.L. Wang, and Y.Q. Jin, "Postearthquake building damage assessment using multi-mutual information from pre-event optical image and postevent SAR image," *IEEE Geoscience and Remote Sensing Letters*, 9(3), pp. 452–456, 2012.
- [6] H. Gokon, and S. Koshimura, "Mapping of building damage of the 2011 Tohoku Earthquake Tsunami in Miyagi prefecture," *Coastal Engineering Journal*, 54(1), 2012.
- [7] H. Breit, T. Fritz, U. Balss, M. Lachaise, A. Niedermeier, and M. Vonavka, "TerraSAR-X SAR Processing and Products," *IEEE Transactions on Geoscience and Remote Sensing*, 48(2), pp. 727–740, 2010.
- [8] W. Liu, and F. Yamazaki, "Detection of crustal movement from TerraSAR-X intensity images for the 2011 Tohoku, Japan Earthquake," *IEEE Geoscience and Remote Sensing Letters*, DOI: 10.1109/LGRS.2012.2199076, 2012.
- [9] Yahoo! JAPAN. <http://archive.shinsai.yahoo.co.jp/>